Environmental Science Advances

ROYAL SOCIETY OF CHEMISTRY

PAPER

View Article Online
View Journal | View Issue

Cite this: *Environ. Sci.: Adv.*, 2022, **1**, 320

Triptycene-based and imine linked porous uniform microspheres for efficient and reversible scavenging of iodine from various media: a systematic study†

Atikur Hassan, Akhtar Alam, Sohom Chandra, Prince and Neeladri Das *

The effective and efficient capture as well as storage of radioisotopes of iodine is of significant importance in the treatment of nuclear waste. Further, the use of radioisotopes of iodine in medical therapy requires proper capture of radioactive iodine. Thus, there is a pressing need to develop novel adsorbents obtained using easy and simple methods that can capture iodine from various media with good uptake capacity. With this target, a new triptycene-based porous organic network (**TP_POP-7**) was designed and synthesized using a flexible trialdehyde with a triazine core and a rigid three-dimensional triptycene triamine as monomers. The two trifunctional monomers were covalently linked using the Schiff base reaction. **TP_POP-7** is a porous organic polymer with good thermal and chemical stability. Due to the presence of abundant electron rich arene rings and N centers in the polymeric framework, efficient interaction with iodine was anticipated. Indeed, **TP_POP-7** proved to be a promising material for capturing iodine from various media/conditions such as iodine vapor at elevated temperature (75 °C: 4215 mg g^{-1}) and room temperature (25 °C: 2040 mg g^{-1}), iodide ions from aqueous solution (2312 mg g^{-1}) and molecular iodine from organic solution (865 mg g^{-1}). Further, **TP_POP-7** is a recyclable adsorbent without much compromise in its capture performance. Considering the high iodine uptake values under different conditions with good retention capability, **TP_POP-7** emerges as one of the best materials for reliable capture and storage of iodine.

Received 5th February 2022
Accepted 30th May 2022

DOI: 10.1039/d2va00024e

rsc.li/esadvances

Environmental significance

Nuclear energy power plants are associated with negligible greenhouse gas emissions during the course of their life span, relative to thermal power plants. Although nuclear plants are the best alternative energy sources to combat global warming, the simultaneous generation of nuclear waste and its inadvertent leakage into the ecosystem is a significant environmental risk. In nuclear waste and spent fuel, the presence of certain isotopes of volatile iodine (^{129}I and ^{131}I) is a major concern due to their high mobility and radiotoxicity. Thus, development of porous materials for efficient trapping of iodine species has acquired considerable significance. Presented herein is a triptycene-based recyclable POP for rapid and high uptake of iodine species from various media.

Introduction

In the contemporary world, developed nations have started relying, to a reasonable extent, on nuclear power plants to meet their ever increasing demand for electrical energy.[1] This is because of the global apprehensions about the energy crisis which are inevitable due to the depletion of coal reserves. Further, the use of coal to generate electricity in thermal power plants is associated with the increasing concentration of atmospheric carbon dioxide – a major greenhouse gas that is held responsible for global warming, ocean acidification and other related environmental concerns.[2] In contrast, power plants that generate electricity using nuclear energy have a much lower carbon footprint than those that rely on coal.[3] In spite of the high energy output from nuclear power plants, these are linked with the generation of several radioactive and volatile species (^{14}C, ^{129}I, ^{131}I, ^{3}H, ^{85}Kr and others) during operation.[4,5] Among these gaseous and radioactive fission products, ^{129}I is quite harmful as a pollutant since it emits beta and gamma radiations and has a half-life that is greater than 15 million years.[6] ^{131}Iodine is another radioisotope of iodine that is released in the environment in the unfortunate event of a nuclear plant accident.[7,8] ^{131}I has a much shorter half-life (~8 days) and it is often used in radiation therapy to treat thyroid cancer.[9] Since thyroid glands concentrate iodine to produce thyroxine, inhalation of radioisotopes of iodine may introduce radioactive isotopes in the metabolic system and cause

Department of Chemistry, Indian Institute of Technology Patna, Patna 801106, Bihar, India. E-mail: neeladri@iitp.ac.in; neeladri2002@yahoo.co.in; Tel: +91-9631624708

† Electronic supplementary information (ESI) available. See https://doi.org/10.1039/d2va00024e

radiation poisoning and thyroid cancers in healthy individuals.[10,11] Toxic radioiodine vapors are also present in off-gas streams due to the processing of nuclear waste and their release into the atmosphere would have serious detrimental effects on the environment.[12] Furthermore, in the unfortunate incidents of nuclear plant accidents, a potential environment threat is the inevitable release of radioactive isotopes of iodine into the surroundings.[13] Indeed, according to the data of a recent survey around the site of Fukushima nuclear power plant, a relatively large amount of radioactive iodine was discharged into the environment compared to other radioactive nuclides.[14,15] This is primarily because of the volatile nature of the element iodine. Considering these above-mentioned facts, there is a need to address these environmental concerns by developing novel porous adsorbent materials that can efficiently capture radioiodine generated from various sources and present in various media such as air, water and other solvents.[7,16]

Presently, radioiodine nuclei are captured mainly *via* chemisorption by using either sorbents coated/impregnated with silver salts or corrosive caustic/acidic solutions.[17,18] The associated disadvantages are high capital costs, equipment fouling, relatively low uptake capacities, decomposition of AgX substrates, loss of silver during regeneration and others.[19,20] More recently, physisorption is being explored as a viable technique to remove radioactive iodine contaminants.[21] This method (physisorption) is gaining importance since it has higher capture efficiency.[22] Further, iodine removal by physisorption is eco-friendly in nature, cost-effective and involves a simplistic method of operation.[23] In this context, traditional porous materials such as activated carbons, zeolites, and advanced porous materials such as metal–organic frameworks (MOFs) have been explored as adsorbents for iodine capture and storage.[7,16,24,25] Apart from these materials, nanomaterials based on Cu/Au have also been explored for iodine capture.[26,27] However, the slow iodine uptake capacity and low physicochemical stability of these above-mentioned adsorbents have limited their practical applicability.[28] Consequently, porous organic polymers (POPs) have recently drawn attention as potential adsorbents for iodine capture and storage purpose.[3,29]

POPs are a class of porous materials that are obtained exclusively from organic building blocks.[30] Due to the absence of metals, unlike MOFs,[31] these have low skeletal density and are associated with high surface area and porosity.[32,33] POPs have ample active sites and these can be easily functionalized to tune their properties.[34,35] A judicious choice of monomers yields POPs in high yield *via* facile reactions that include but are not limited to metal catalyzed cross-coupling and condensation polymerization.[36–40] Among the various methodologies, Schiff base condensation is a very simple and efficient reaction to synthesize imine linked POPs that have wide applications in the fields of gas storage, catalysis, biology, energy, environmental remediation and so on.[41–43] A literature survey indicated that only a few imine-linked POPs have been explored to date as strategic materials for iodine capture and storage purpose.[16,44–47] Moreover, the capture capacities of such imine-linked POPs are reported to be moderate in spite of the fact that these porous networks are rich in nitrogen centers and have ample aromatic sites.[47–50] Further, the pore size and surface area of the imine-linked POPs may be suitably changed by incorporating plenty of structural motifs that have π-conjugated units. This assists in improving their porous properties and makes them promising agents for effective removal of radioiodine that may be present in various media.[12,51] In this perspective, we envisioned the design of a new imine-linked POP (**TP_POP-7**) with plentiful π-rich arene motifs using the cost-effective Schiff base polycondensation reaction. It was anticipated that such a network POP (**TP_POP-7**) could be easily obtained by reacting a nitrogen rich as well as flexible trialdehyde and a tri-amine derivative of triptycene as monomers. Nitrogen centers in the polymeric backbone are known to improve the adsorbent's affinity towards iodine.[49,50] On the other hand, the intentional inclusion of triptycene units was expected to provide the required rigidity to the skeletal framework, thereby imparting high physicochemical stability to the resultant POP.[37,52–57] Moreover, this synthetic strategy (to obtain the iodine adsorbent – **TP_POP-7**) would be economical relative to the previously reported POPs for iodine capture that were obtained by employing transition metal-catalyzed cross coupling reactions.[58–61] After successful synthesis, **TP_POP-7** was characterized using various analytical techniques. **TP_POP-7** was found to be chemically stable and subsequently it was tested as an adsorbent for iodine removal in the vapor phase, at elevated as well as ambient temperature, from water and an organic solvent (*n*-hexane). Experimental data indicate that **TP_POP-7** is an effective adsorbent and these results are discussed in the ensuing sections.

Experimental section

Materials and instrumentation

All the chemicals and reagents were procured locally. More details related to chemicals (used for synthesis) and instruments (used for characterization and analysis) are mentioned in ESI page S-3.†

Synthesis of monomers and TP_POP-7

The detailed synthetic procedures to obtain the precursor molecules (**TCA** and **TP-NH$_2$** used as monomers) and **TP_POP-7** are mentioned in the ESI† (page no. S-4 to S-7 and NMR spectra in Fig. S1–S4†).

Results and discussion

Briefly describing the syntheses of the monomers used to obtain **TP_POP-7**, these can be easily prepared from economical and commercially available compounds such as triptycene, 4-hydroxybenzaldehyde and cyanuric chloride. **TP_POP-7** was obtained *via* a solvothermal reaction of compounds **1** (triazine core aldehyde: **TCA**) and **2** (2,6,14-triaminotriptycene: **TP-NH$_2$**) dissolved in a mixture of dioxane and mesitylene (1 : 1 v/v) along with 3 M acetic acid at 120 °C for 72 hours (Scheme 1).

After 72 hours of reaction, an off-white precipitate was obtained that was filtered off and washed with copious amounts of

Scheme 1 Synthesis of TP_POP-7.

solvents such as DMF, THF, and methanol. Further purification required the use of a Soxhlet extractor such that impurities were extracted in a mixture of hot THF and methanol. The obtained product (**TP_POP-7**) was dried at 100 °C overnight and used subsequently for characterization using the commonly available techniques. Fourier-transform infrared (FT-IR) spectroscopy was primarily used to investigate the formation of covalent linkages between the monomers in the obtained product. The FT-IR spectra of the arene monomers and **TP_POP-7** are shown in Fig. 1a. In the FT-IR spectrum of **TP_POP-7**, the appearance of a strong new peak centered at 1572 cm^{-1} was an indication of the successful linkage of the monomers *via* imine bonds that are associated with large changes in dipole moments. The characteristic primary amine bands (in the range of 3300–3500 cm^{-1}) observed in the **$TP\text{-}NH_2$** monomer and the sharp carbonyl band in TCA (1700 cm^{-1}) are absent in the product

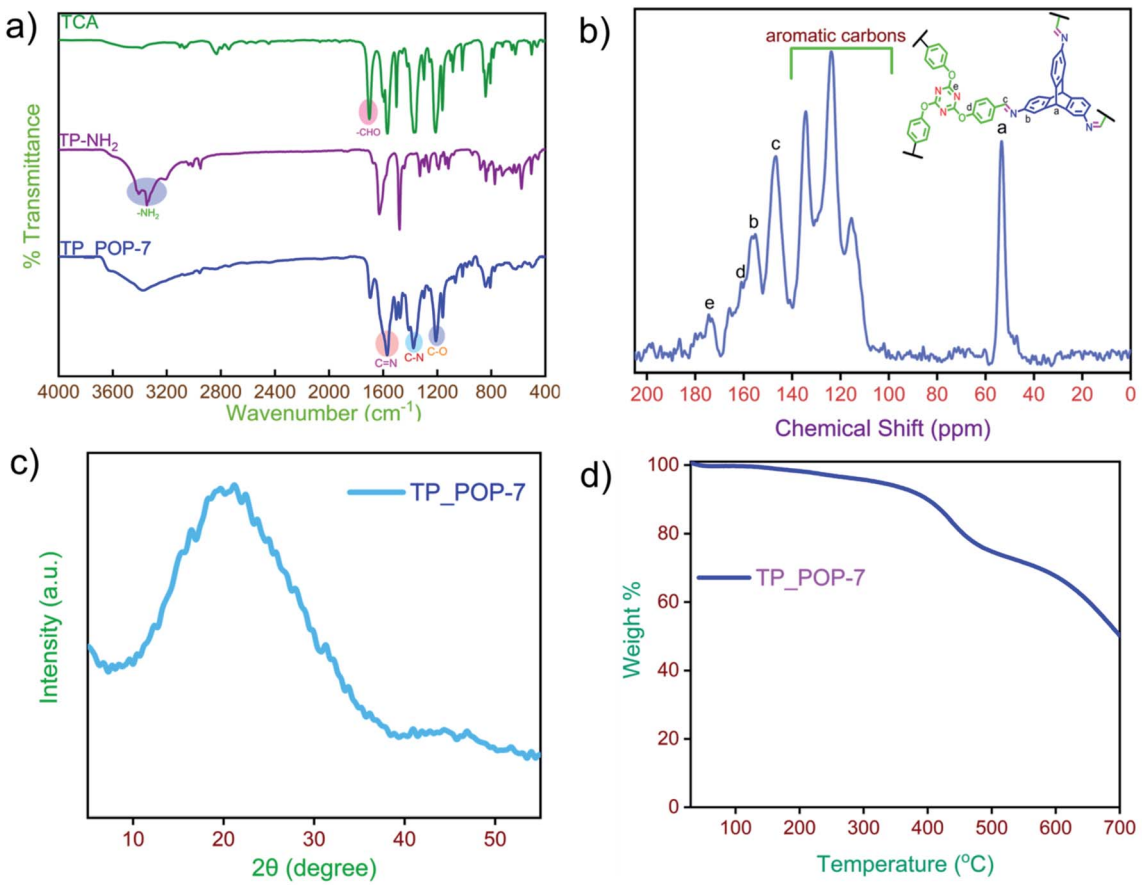

Fig. 1 Structural characterization of **TP_POP-7**: (a) FT-IR spectra of **TP_POP-7** with the corresponding monomers. (b) Solid-state ^{13}C CP-MAS NMR spectra of **TP_POP-7**. (c) PXRD plot of **TP_POP-7**. (d) TGA analysis of **TP_POP-7**.

which also supports successful polymerization as shown in Scheme 1.[62] Additionally, the bands centered at 1363 and 1208 cm^{-1} in the FT-IR spectrum of **TP_POP-7** are assigned to the stretching vibrations of C–N and C–O bonds in this material, thereby confirming the incorporation of triptycene and triazine structural motifs in its polymeric framework.

TP_POP-7 is not soluble in common organic solvents (Table S1†). Thus, solid-state ^{13}C CP-MAS NMR was used to investigate the carbon environment of **TP_POP-7** at the molecular level (Fig. 1b). In the ^{13}C NMR spectrum, the peak centered at 146 ppm is due to the carbon associated with the imine bond. The signal at 55 ppm is attributed to the bridgehead carbon of the triptycene unit which also confirms the successful incorporation of triptycene motifs in the obtained polymeric network.[63] The chemical shifts observed in the region of 100–130 ppm correspond to the carbon nuclei of the arene rings present in **TP_POP-7**. The signal at 174 ppm indicates the incorporation of triazine rings in the polymeric backbone.[64] To check the crystalline nature of **TP_POP-7**, powder X-ray diffraction (PXRD) analysis (Fig. 1c) was performed. The absence of any sharp diffraction peaks in the XRD pattern confirms its amorphous nature. Moreover, the appearance of a broad peak between 20 and 30 (2θ) degrees is possibly due to the π–π stacking of arene rings.[65]

Furthermore, the thermal stability of **TP_POP-7** was investigated by thermogravimetric analysis (TGA) which was performed in the temperature range of 30 °C to 700 °C and in a nitrogen atmosphere. The TGA plot of **TP_POP-7** shows that the material is quite stable up to 350 °C and at 700 °C, more than 50% of the mass is retained (Fig. 1d). The observed thermal stability is due to the inclusion of robust and rigid triptycene units in the polymeric framework.

The porous properties of the as-synthesized **TP_POP-7** were examined by collecting N_2 adsorption and desorption isotherms at 77 K. Prior to gas uptake experiments and related analysis, **TP_POP-7** was thoroughly activated at 120 °C. In the region of low surface coverage ($P/P_0 < 0.05$), there was a rapid nitrogen gas uptake, which indicated the presence of micropores in the organic network of **TP_POP-7**. At relatively high P/P_0, the N_2 uptake trend suggests the presence of mesopores. The N_2 sorption isotherm is depicted in Fig. 2a and it can be categorized as a type-II isotherm.[66] The surface area of **TP_POP-7** was calculated using the BET model and it was found to be 86 $m^2\ g^{-1}$. The corresponding BET plot is shown in Fig. S5.† The pore size distribution of **TP_POP-7** (Fig. 2b) was calculated using the non-local density functional theory (NLDFT method). The pore volume, based on the NLDFT method, was found to be 0.097 $cm^3\ g^{-1}$.

It is important to gain the morphological information of a newly reported as-synthesized material. Therefore, the FE-SEM micrographs of **TP_POP-7** were recorded at various magnifications and are shown in Fig. 2c and d and S6.† A

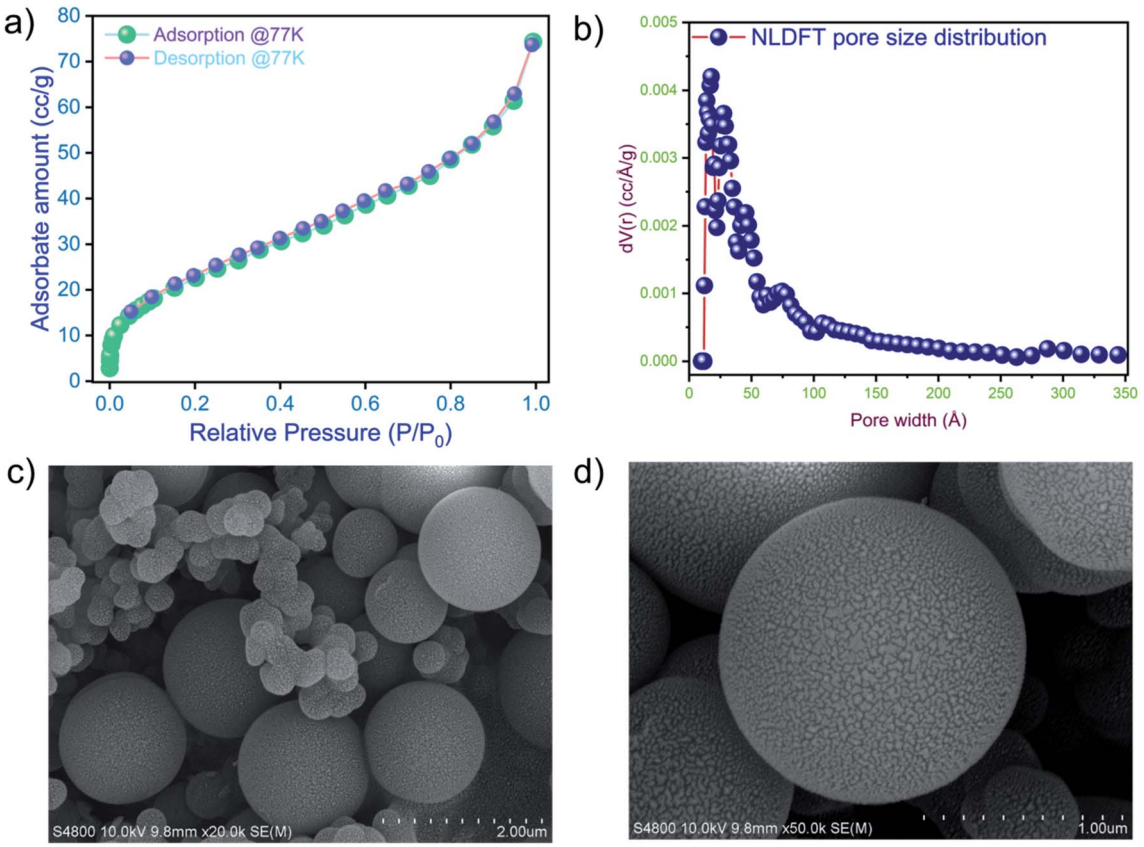

Fig. 2 (a) Low-temperature (77 K) N_2 adsorption/desorption isotherms of **TP_POP-7**. (b) PSD curve of **TP_POP-7**. (c and d) FESEM images of **TP_POP-7**.

spherical morphology was seen at different magnifications, which indicates the smooth progress of the reaction. EDX analysis of pristine **TP_POP-7** shows the presence of C, N, and O elements (Fig. S7†). Further, we also performed DLS experiments to determine the particle size distribution in **TP_POP-7**. DLS data indicated a bimodal size distribution of particles in the network of **TP_POP-7** (Fig. S8†). To check the chemical stability of **TP_POP-7**, a few milligrams of the material were placed separately in 4 M HCl and 6 M NaOH solutions. The polymeric materials were collected by filtration from both solutions after three days and then characterized by recording their FT-IR spectra. Comparison of the FT-IR spectra of the treated material (Fig. S9†) with those of the pristine (as synthesized) material indicated that there were no noticeable changes. This observation hinted at the good chemical stability of the imine linkages present in **TP_POP-7** under the testing conditions.

TP_POP-7 has a porous structure that has abundant N-rich sites along with ample aromatic rings. In addition, **TP_POP-7** shows good thermal/chemical stability which enthused us to carry out iodine capture experiments. In these studies, the stable isotope (^{127}I) was used as a surrogate of radioactive iodine (^{129}I and ^{131}I) since these isotopes have nearly identical chemical properties.[67] Iodine vapor sorption studies of **TP_POP-7** were performed using gravimetric measurement at 75 °C and ambient pressure and these conditions mimic closely the nuclear fuel reprocessing settings[23,59,62] (details of the experimental procedure are given in page no. S-11 and S-12†).

A sample of **TP_POP-7** was first activated and then weighed in a small glass vial. This small vial was placed inside a larger vial to avoid direct surface contamination during the iodine uptake experiments. This set-up was then placed in a sealed glass chamber containing iodine granules at the bottom. Next, the sealed glass container was placed in a preheated oven maintained at 75 °C under ambient pressure. The iodine uptake by **TP_POP-7** was recorded at different intervals of time. The result indicated that during the adsorption process, the iodine uptake increases rapidly in the first 12 hours and later reaches a plateau (Fig. 3a). An obvious color change from off-white to dark brown was observed (Fig. 3d). After 36 hours, no major mass increase was noted in the sample of **TP_POP-7** which suggested that the sample had reached its highest adsorption capacity within this time frame. In order to verify that the **TP_POP-7** sample had attained the equilibrium adsorption capacity, the experiment was continued up to 48 hours. Results indicated that the given sample of **TP_POP-7** was saturated with iodine within approximately 36 hours. The equilibrium iodine uptake capacity was found to be 4.215 g g^{-1}. To the best of our knowledge, the iodine uptake capacity of **TP_POP-7** is not the highest but it is one of the highest values among the vast domain of porous iodine adsorbents reported to date (comparison shown in Table S2†). Under similar settings, a control experiment was performed without the **TP_POP-7** adsorbent. No change of mass was observed in the glass vial with gradual passage of time which confirmed that the iodine vapors were actually captured by **TP_POP-7** in the previous

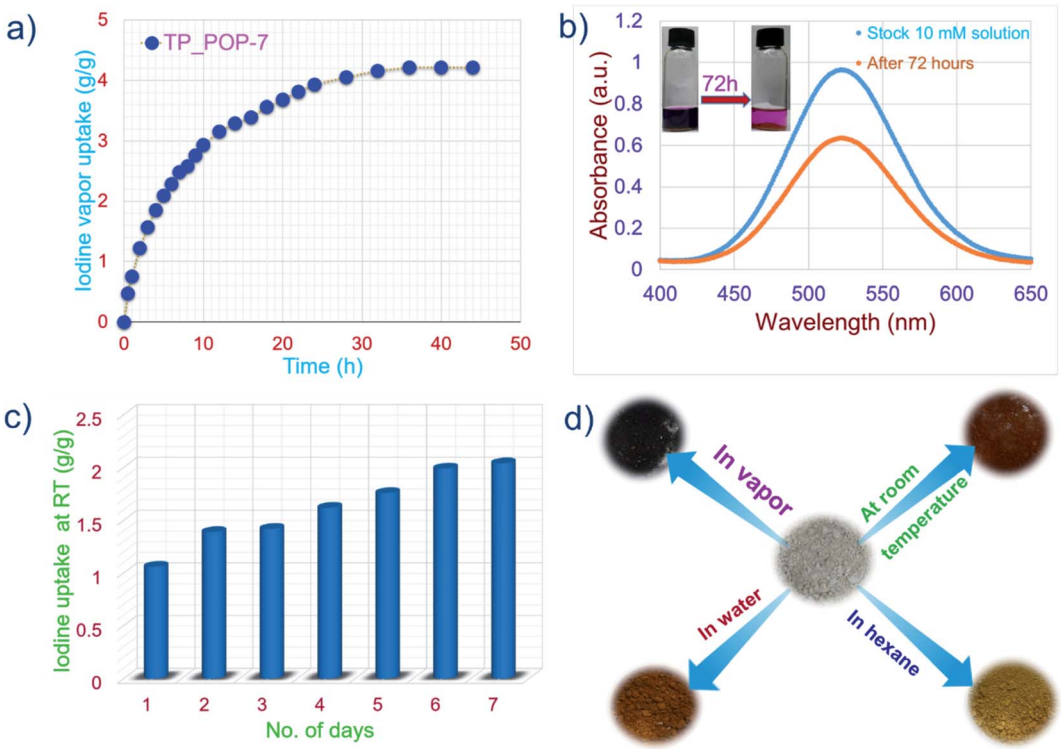

Fig. 3 (a) Iodine uptake curve of **TP_POP-7** in the vapor phase at 75 °C. (b) Capture capacity plot of **TP_POP-7** in hexane. (c) Iodine uptake at room temperature. (d) Digital images of **TP_POP-7** before and after iodine capture in various media.

experiment. Next, we also performed kinetics experiments of iodine capture and it was concluded that the gravimetric iodine capture experiments follow pseudo-second order kinetics (Fig. S10†).

Subsequently, using a sample of I_2@TP_POP-7, experiments were also performed to test the retention capacity of **TP_POP-7**. At different intervals of time, I_2@TP_POP-7 exposed to air and under ambient conditions did not show any significant weight loss (Fig. S11†). This suggested a good iodine retention ability of **TP_POP-7** and hence justifies its potential to act as an adsorbent of radioactive iodine in unfortunate events of nuclear accidents. Furthermore, the iodine capture capability of **TP_POP-7** was tested by exposing it to iodine vapor at room temperature. Such an experiment is important since the highly radioactive iodine (^{131}I) may be present in the environment due to its release in the aftermath of a nuclear accident. Therefore, an adsorbent designed for practical applications should also be able to efficiently capture iodine at ambient temperature (25 °C). To test **TP_POP-7** under these conditions, the polymer sample with a known weight was placed inside a smaller vial that was in turn placed inside a bigger glass containing a few granules of iodine. Iodine slowly sublimed at ambient temperature and the vapors (of iodine) were adsorbed on the porous surface of **TP_POP-7**. The increase in weight of the **TP_POP-7** sample was measured at an interval of 24 h for up to 7 days (Fig. 3c). The equilibrium uptake capacity of iodine was recorded to be 2.04 g g^{-1} after 7 days, beyond which no significant increase in weight of the **TP_POP-7** sample was observed. This implied that the **TP_POP-7** sample reached equilibrium uptake of iodine in 7 days under the experimental conditions. Visually, as each day elapsed, we witnessed a noticeable change in the color of **TP_POP-7** from off-white to darker shades and eventually deep brown (Fig. 3d). To the best of our knowledge, this magnitude of iodine capture at ambient temperature is one of the highest among the previously reported adsorbents (comparison table shown in the ESI: Table S3†). The good results obtained in the experiments related to capture of iodine vapor by **TP_POP-7** (at 75 °C and ambient temperature) prompted us to explore its ability to capture iodine species that may be present in water. Iodine is classified as a hazardous pollutant by the US EPA and as a water pollutant, specifically a class 1 hazard, as per the German Federal Water Management Act. Harmful isotopes of iodine may also be released accidentally into water bodies during nuclear fuel reprocessing or as a medical waste.[68] So, it was our interest to extract iodine species from water. A test solution was prepared by dissolving non-radioactive iodine and KI in water. First, kinetics experiments were performed to evaluate the adsorption kinetics of **TP_POP-7** (Fig. 4a). **TP_POP-7** was able to remove more than 90% of iodine species from aqueous solution within 1 hour and equilibrium was achieved within 2 hours (Fig. 4c). These results suggest that the rate of adsorption of iodine by **TP_POP-7** was very fast and that this polymer may prove to be an excellent candidate as an adsorbent of iodine species from water. Detailed analysis indicated that the adsorption kinetics follows a pseudo second-order kinetics model with the correlation coefficient value $R^2 = 0.999$ (Fig. S12†).

Next, the adsorption isotherms were recorded and the corresponding data are shown in Fig. 4e and S13a.† The correlation coefficient value showed a better fit with a Langmuir adsorption model than with the Freundlich model. Thus, we conclude that iodine uptake by **TP_POP-7** from water involves monolayer formation of the adsorbate on the surface of the adsorbent. To evaluate the maximum iodine adsorption capacity, 50 mg of an activated sample of **TP_POP-7** was added to an aqueous solution (3 ml) of 600 mg KI and 300 mg I_2. The maximum iodine adsorption capacity of **TP_POP-7** was recorded to be 2312 mg g^{-1} which was also verified by sodium bisulfate titration. It is worth noting that the observed iodine loading capability of **TP_POP-7** is much higher than that of other previously reported porous sorbents in recent literature (comparison shown in Table S4†).

Next, it was our interest to assess the ability of **TP_POP-7** to capture iodine dissolved in organic solvents such as hexanes. Iodine dissolved in a non-polar solvent (such as *n*-hexane or cyclohexane) yields a violet colored solution. Iodine entrapment by **TP_POP-7** was monitored by recording the UV-Vis spectra of the hexane solution of iodine at different intervals of time (Fig. 4b). With the gradual progress of time, the intensity of the violet color decreased and this was evident from the decrease in the magnitude of the absorption maxima in the UV-Vis spectra. Data suggested that **TP_POP-7** captured more than 80% of iodine from the hexane solution (Fig. 4d). We performed kinetics experiments to obtain useful information related to the kinetics of iodine capture by **TP_POP-7** from hexane, and it was observed that the data fitted well with a pseudo-second order kinetics model since the corresponding correlation coefficient value indicates better fitting (Fig. S14†). Additionally, to understand the mode of iodine capture by **TP_POP-7** from hexane solution, isotherm model studies were performed with different concentrations of solutions. The data obtained from adsorption isotherms were fitted with Langmuir and Freundlich isotherm models. It was observed that the data fitted better with the Langmuir model (Fig. 4f and S13b†). To determine the maximum adsorption capacity, 10 mg of **TP_POP-7** was suspended in 10 ml of iodine solution (10 mM) (Fig. 3b). The maximum adsorption capacity was found to be 865 mg g^{-1} and this magnitude is comparable or even superior to the performance of various previously reported sorbents (comparison shown in Table S5†). Subsequently, it was our curiosity to understand the mechanism of iodine capture by **TP_POP-7**. For this purpose, samples of **TP_POP-7** loaded with iodine (I_2@TP_POP-7) were studied using various analytical techniques such as FT-IR, FE-SEM, EDX, TGA, Raman spectroscopy and XPS analysis. Fig. 5a shows the comparison of FT-IR spectra of **TP_POP-7** before and after iodine capture in which shifts in the characteristic peak positions were clearly observed. Briefly, the bands due to C=N (1572 cm^{-1} → 1563 cm^{-1}) and C–N (1208 cm^{-1} → 1203 cm^{-1}) stretching vibrations in the pristine material shifted upon iodine uptake. These observed changes in the FT-IR spectra imply that the arene rings (including triazine) and the nitrogen centres act as binding sites for iodine molecules. The small shift in the peaks also suggests weak interactions due to the physisorption of iodine on the surface of

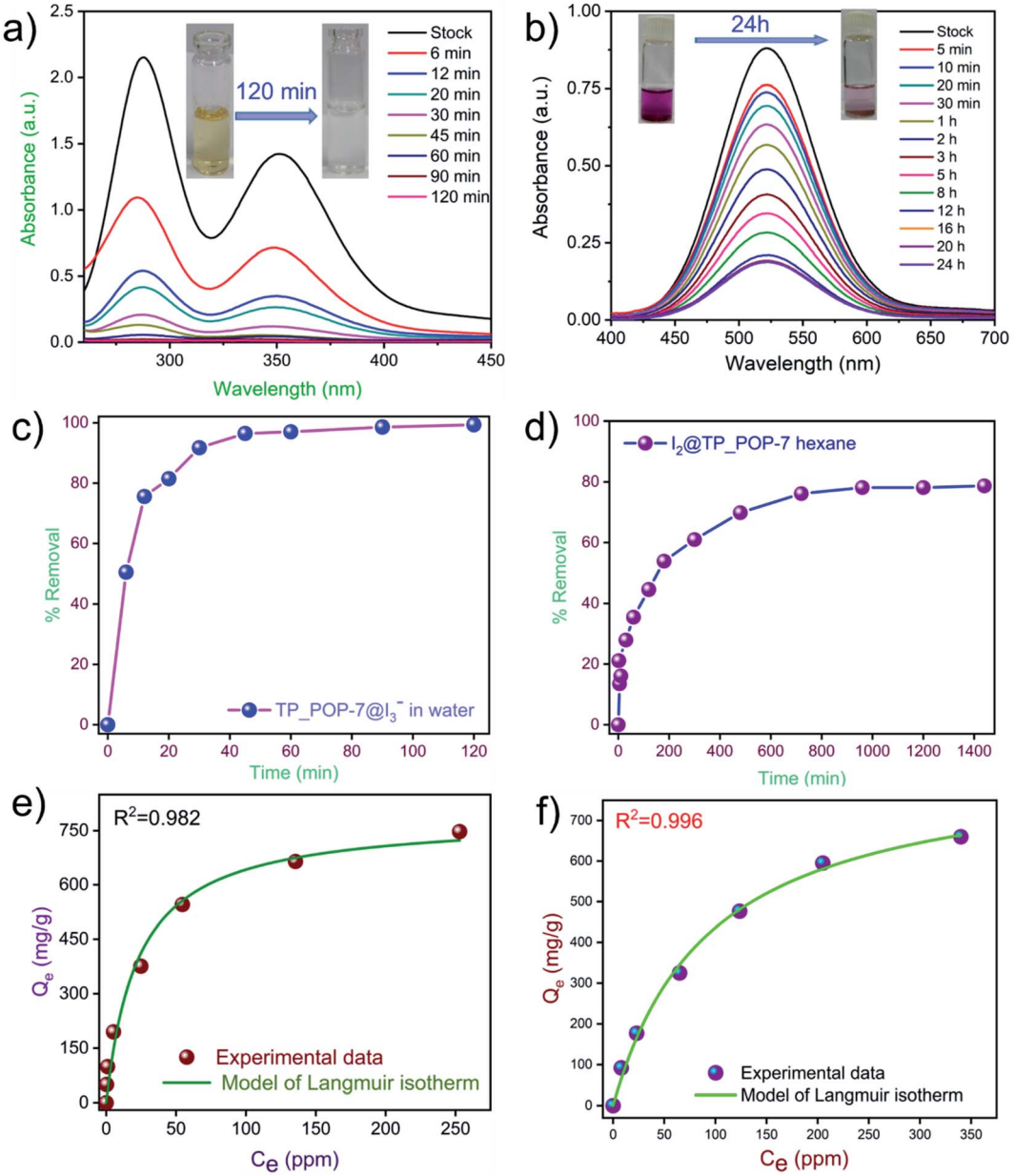

Fig. 4 (a) UV-Vis spectra of iodine capture from aqueous solutions by **TP_POP-7** at different time intervals. (b) UV-Vis spectra showing gradual uptake of iodine dissolved in hexane by **TP_POP-7** at different time intervals. (c) Extent of iodine captured by **TP_POP-7** from aqueous solutions at various time intervals. (d) Extent of iodine captured by **TP_POP-7** from hexane solutions at various time intervals. (e) Langmuir isotherm fitting for iodine capture by **TP_POP-7** from aqueous solution. (f) Langmuir isotherm fitting for iodine capture by **TP_POP-7** from hexane solution.

TP_POP-7. Further, noticeable visual morphological changes were observed upon comparing the FE-SEM images of **TP_POP-7** and I_2@TP_POP-7 (Fig. 5b and S15†). Specifically, on a closer analysis, small islands that appeared on the spherical aggregates of **TP_POP-7** were absent on the microspheres of I_2@TP_POP-7. We speculate that this visible change may be due to the deposition of iodine on the surface of **TP_POP-7**.

This fact was also supported by the EDX analysis of a sample of I_2@TP_POP-7. The EDX data revealed high iodine content as shown in Fig. 5c. Furthermore, the TGA analysis (N_2 atmosphere) of I_2@TP_POP-7 shows a gradual weight loss in the temperature range of 70–400 °C. The weight loss is due to the release of the adsorbed iodine from I_2@TP_POP-7 (Fig. S16†). Raman spectroscopy was used to obtain insight on the nature of iodine species present in I_2@TP_POP-7. As shown in Fig. S17,† no sharp peak was observed in pristine **TP_POP-7** due to the absence of iodine species. However, for I_2@TP_POP-7, a highly intense peak at 167 cm^{-1} was observed. This signal corresponds to the presence of polyiodide species of iodine.[69] It is proposed that the nitrogen rich C=N linkages and the aromatic arene rings present in the polymeric framework in **TP_POP-7** can lead to charge transfer complexation with electron deficient iodine species (Fig. 5d).

To obtain more information related to the adsorption of iodine species by **TP_POP-7**, XPS (X-ray photoelectron

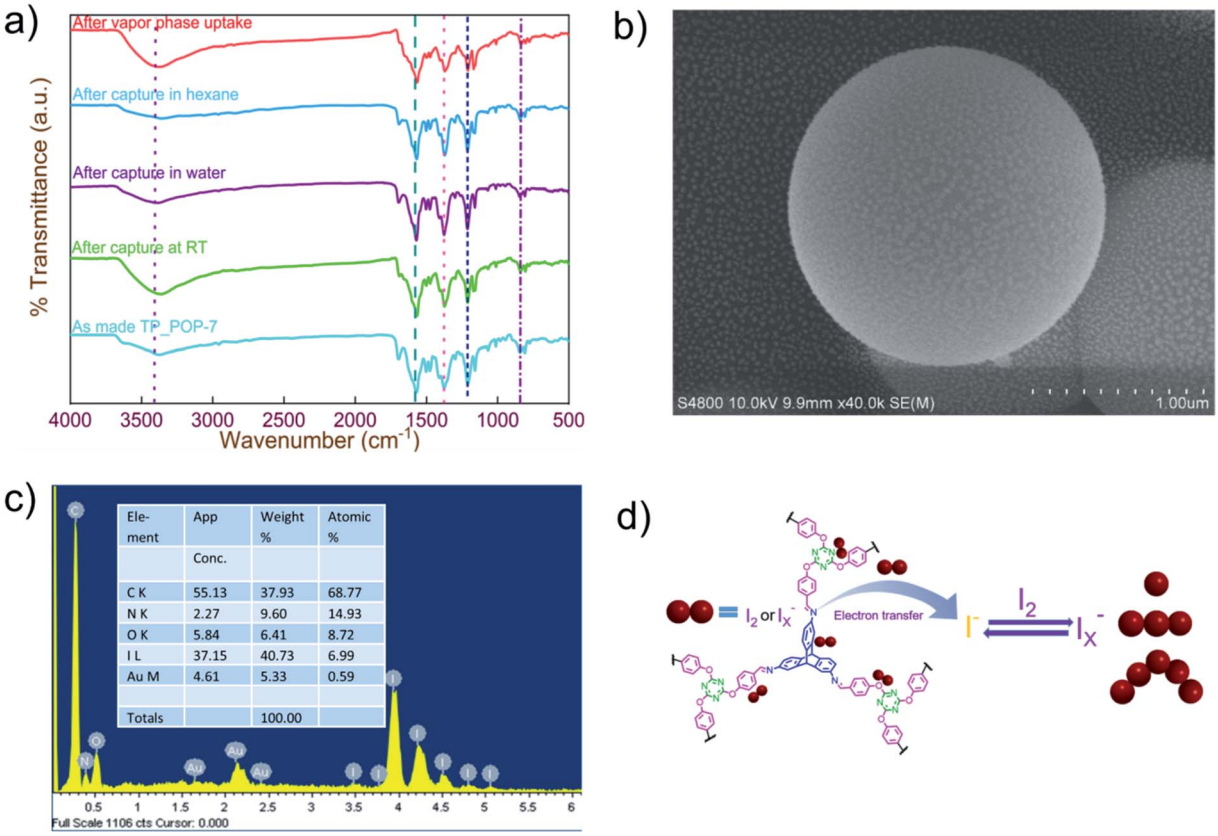

Fig. 5 (a) FT-IR spectra of **TP_POP-7** before and after capturing iodine from different media. (b) FE-SEM image of I_2@TP_POP-7. (c) EDX analysis of I_2@TP_POP-7 and (d) the probable mechanism of iodine capture by **TP_POP-7**.

spectroscopy) data (Fig. 6 and S18†) were recorded for both the pristine polymer and I_2@TP_POP-7 (iodine loaded polymer). The characteristic binding energy peaks for the 3d orbital of iodine were absent in the XPS spectrum (Fig. 6a) of the pristine polymer (**TP_POP-7**). On the other hand, the XPS survey spectrum of I_2@TP_POP-7 indicated the successful capture of iodine species due to the presence of binding energy peaks for the 3d orbital of the element iodine in the range of 615 to 635 eV (Fig. 6b). Here, the two split peaks are assigned to the $3d_{3/2}$ and $3d_{5/2}$ energy levels of iodine centered at 630.73 and 619.28, respectively.[25,47,48,50,72–74] The appearance of a shoulder in each individual split peak indicated the presence of polyiodide species (I_3^- and I_5^-) along with molecular iodine (I_2).[70,71] Furthermore, it was observed (Fig. S18†) that the peak corresponding to the N 1s core level appearing at 398.75 eV in pristine **TP_POP-7** shifted to 399.29 eV in the iodine loaded POP

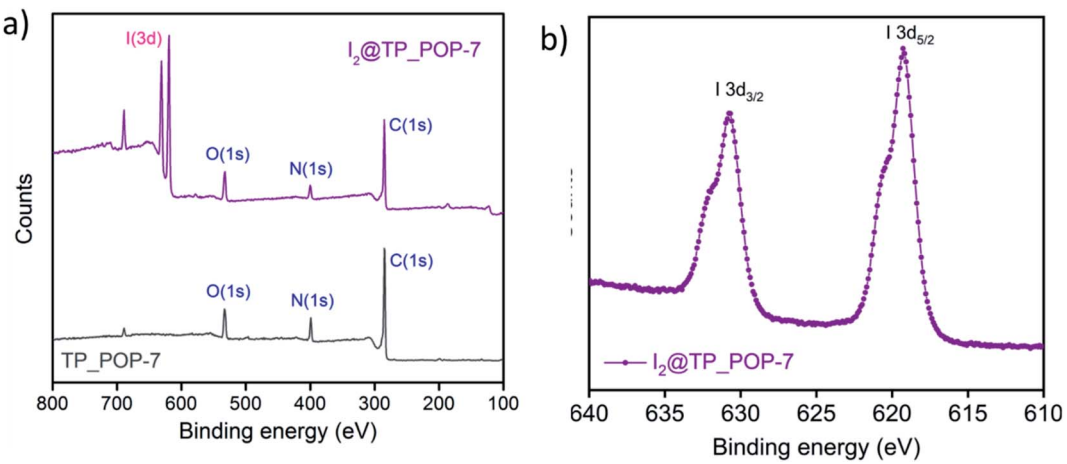

Fig. 6 (a) XPS survey spectra of **TP_POP-7** before and after iodine capture. (b) High resolution XPS spectra of I 3d of I_2@TP_POP-7.

(I_2@TP_POP-7). This clearly indicated the presence of favorable interactions between electron rich N centers (present in the polymeric backbone of **TP_POP-7**) and relatively electron deficient iodine molecules. This observation also ratified the strong affinity of **TP_POP-7** for iodine species which may also be attributed to the presence of ample number of N atoms that interact efficiently through their lone pair with relatively electron poor iodine.[12,44,62,72]

The recovery of iodine from I_2@TP_POP-7 was studied thoroughly by either heating or soaking the sample in polar solvents (detail procedure: page no. S-18). I_2@TP_POP-7 with a known weight was placed in an open vial and heated at 125 °C for 6 hours. Approximately 90% of the captured iodine was released within 2 hours of heating and around 98% of iodine was released in the next 4 hours (Fig. 7a). Complete removal was not achieved because some iodine molecules were trapped in the polymeric network having irregular/non-uniform pore size distribution. Iodine desorption studies were performed by extracting iodine from I_2@TP_POP-7 using two different polar solvents – methanol and DMSO.

In these experiments, a known amount of I_2@TP_POP-7 was placed in a 20 ml glass vial. Next, 15 ml of solvent (either methanol or DMSO) was added and the UV-Vis spectra were recorded at specific time intervals (Fig. 7b and c). With the gradual passage of time, the color of each solvent turned from colourless to light yellow and finally deep yellow (Fig. S19 and S20†). The I_2 released was monitored by UV-Vis spectroscopy for 90 min. A relatively fast release of iodine was observed when DMSO (Fig. S21†) was used as the extracting solvent. On the other hand, the release of iodine in methanol (Fig. S22†) was comparatively slow.[75,76] In the methanol solution, the peaks with absorption maxima at 290 and 358 nm are due to the presence of polyiodide ions which confirms the presence of these iodine species captured on the surface and pores of **TP_POP-7**.[76] Considering from an application point of view, reusability of a material is an important criterion that is desirable in any good adsorbent. Our results indicate that **TP_POP-7** qualifies as a good adsorbent since it can be regenerated easily with the rapid release of most of the captured iodine under ambient conditions.

We were also interested to study the recyclability of **TP_POP-7** as an adsorbent for iodine capture. For this purpose, I_2@TP_POP-7 was heated at 125 °C for 6 hours to release the captured iodine and the regenerated sample of **TP_POP-7** was reused for subsequent cycles of iodine adsorption and desorption. Results indicate that **TP_POP-7** can be recycled several times without any significant loss in performance as an adsorbent (Fig. 7d). As per the experimental data, at the end of the seventh cycle, the regenerated sample of **TP_POP-7** could capture at least 3.9 g g^{-1} iodine. These results prompted us to conclude that **TP_POP-7** is one of the best performing porous adsorbent materials for reliable iodine capture and storage purpose.

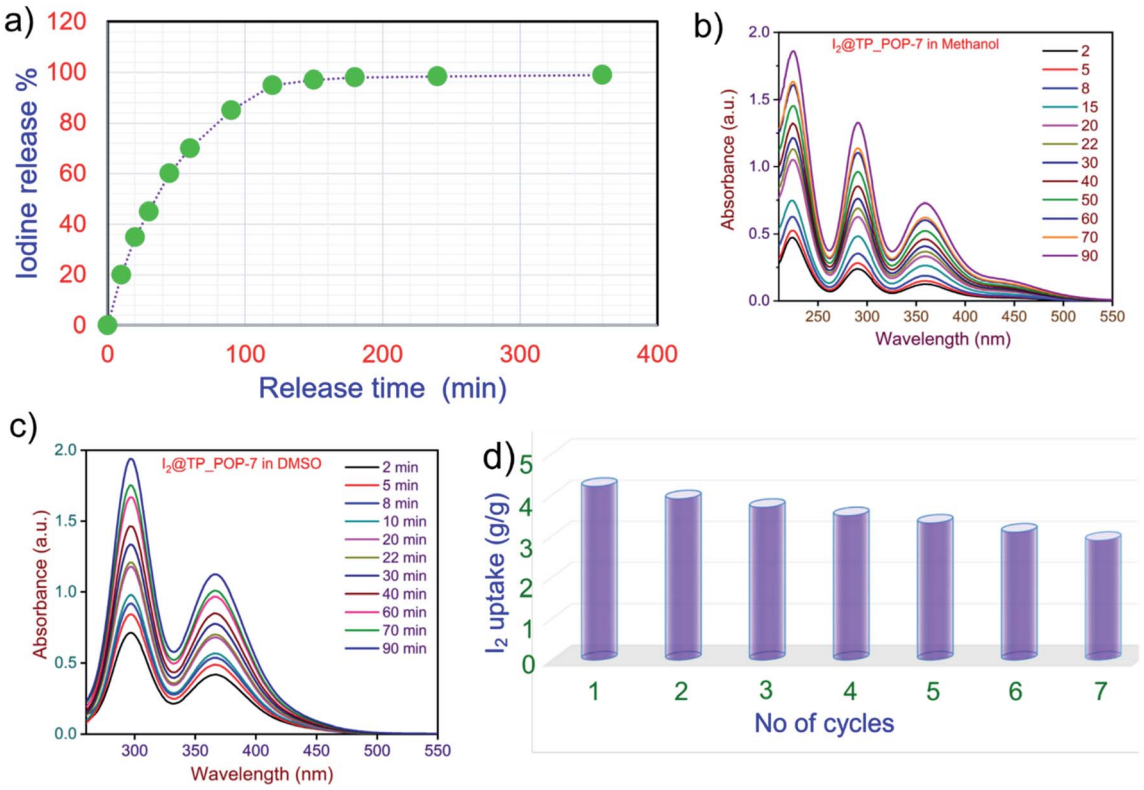

Fig. 7 (a) Iodine release upon heating. (b) Iodine delivery in methanol from I_2@TP_POP-7. (c) Iodine delivery in DMSO from I_2@TP_POP-7. (d) Reusability of TP_POP-7.

Conclusion

A cost-effective and facile synthesis of a triptycene based porous organic polymer (**TP_POP-7**) has been reported that uses an efficient Schiff base polycondensation reaction between triaminotriptycene and a triazine-based trialdehyde, under solvothermal conditions. The obtained **TP_POP-7** was thoroughly characterized using various analytical techniques. The incorporation of lightweight elements, plentiful of nitrogen centers, π-rich arene rings and rigid triptycene motifs impart a moderate physicochemical stability and surface area to the material. The resulting **TP_POP-7** shows excellent iodine adsorption capacity at an elevated temperature (75 °C: 4215 mg g^{-1}) and room temperature (25 °C: 2040 mg g^{-1}), from aqueous solution (2312 mg g^{-1}) and organic solution (865 mg g^{-1}). The iodine capture capacity of **TP_POP-7** from various media is comparable or even superior to that of several porous materials previously reported in the scientific literature. The iodine capture mechanism was thoroughly studied using additional experiments including XPS and Raman spectroscopy. Further, **TP_POP-7** can be reused up to seven cycles for capture and storage of radioactive iodine without much compromise in capture performance. To summarize, we report herein a novel porous organic polymer in the form of **TP_POP-7** that can capture both volatile iodine species, iodide anions and molecular iodine at room temperature. Such characteristics are desirable in an adsorbent for trapping radioactive iodine in the pretreatment of biomedical waste before its proper disposal. Further **TP_POP-7** may find application in nuclear fuel reprocessing where it is essential to capture radioactive iodine under wet conditions. We anticipate that our work will motivate others to synthesize new cost-effective porous organic polymers for capture of various volatile radioactive by-products. This can also contribute to the future growth of the nuclear industry. Research is in progress in our laboratory on similar lines.

Conflicts of interest

There are no conflicts to declare.

Acknowledgements

N. Das, S. Chandra and Prince thank the Indian Institute of Technology Patna (IIT Patna) for providing research infrastructure and instrumental facilities. A. Hassan and A. Alam thankfully acknowledge IIT Patna for their respective Institute Research Fellowships. The authors acknowledge S. Fajal, M. Rahman and S. Kumar for valuable suggestions and discussions during manuscript preparation. The authors also acknowledge the reviewers for their valuable inputs.

References

1 L. Wang, Z. Li, Q. Wu, Z. Huang, L. Yuan, Z. Chai and W. Shi, *Environ. Sci.: Nano*, 2020, **7**, 724–752.
2 G. Singh, J. Lee, A. Karakoti, R. Bahadur, J. Yi, D. Zhao, K. AlBahily and A. Vinu, *Chem. Soc. Rev.*, 2020, **49**, 4360–4404.
3 Q. Sun, B. Aguila and S. Ma, *Trends Chem.*, 2019, **1**, 292–303.
4 X. Zhang and Y. Liu, *Environ. Sci.: Nano*, 2020, **7**, 1008–1040.
5 N. Baig, S. Shetty, S. Al-Mousawi and B. Alameddine, *Polym. Chem.*, 2020, **11**, 3066–3074.
6 B. K. Singh, M. A. Hafeez, H. Kim, S. Hong, J. Kang and W. Um, *ACS ES&T Engg.*, 2021, **1**, 1149–1170.
7 K. Jin, B. Lee and J. Park, *Coord. Chem. Rev.*, 2021, **427**, 213473.
8 R. C. Moore, C. I. Pearce, J. W. Morad, S. Chatterjee, T. G. Levitskaia, R. M. Asmussen, A. R. Lawter, J. J. Neeway, N. P. Qafoku, M. J. Rigali, S. A. Saslow, J. E. Szecsody, P. K. Thallapally, G. Wang and V. L. Freedman, *Sci. Total Environ.*, 2020, **716**, 132820.
9 D. F. Sava, M. A. Rodriguez, K. W. Chapman, P. J. Chupas, J. A. Greathouse, P. S. Crozier and T. M. Nenoff, *J. Am. Chem. Soc.*, 2011, **133**, 12398–12401.
10 I. J. Nixon, J. P. Shah, M. Zafereo, R. S. Simo, I. D. Hay, C. Suárez, P. Zbären, A. Rinaldo, A. Sanabria, C. Silver, A. Mäkitie, V. Vander Poorten, L. P. Kowalski, A. R. Shaha, G. W. Randolph and A. Ferlito, *Eur. J. Surg. Oncol.*, 2020, **46**, 754–762.
11 M. Huang, L. Yang, X. Li and G. Chang, *Chem. Commun.*, 2020, **56**, 1401–1404.
12 L. He, L. Chen, X. Dong, S. Zhang, M. Zhang, X. Dai, X. Liu, P. Lin, K. Li, C. Chen, T. Pan, F. Ma, J. Chen, M. Yuan, Y. Zhang, L. Chen, R. Zhou, Y. Han, Z. Chai and S. Wang, *Chem*, 2021, **7**, 699–714.
13 C. Pei, T. Ben, S. Xu and S. Qiu, *J. Mater. Chem. A*, 2014, **2**, 7179–7187.
14 G. Steinhauser, A. Brandl and T. E. Johnson, *Sci. Total Environ.*, 2014, **470–471**, 800–817.
15 S. Sarina, A. Bo, D. Liu, H. Liu, D. Yang, C. Zhou, N. Maes, S. Komarneni and H. Zhu, *Chem. Mater.*, 2014, **26**, 4788–4795.
16 W. Xie, D. Cui, S.-R. Zhang, Y.-H. Xu and D.-L. Jiang, *Mater. Horiz.*, 2019, **6**, 1571–1595.
17 C. Cao, S. Chong, L. Thirion, J. C. Mauro, J. S. McCloy and A. Goel, *J. Mater. Chem. A*, 2017, **5**, 14331–14342.
18 B. J. Riley, J. D. Vienna, D. M. Strachan, J. S. McCloy and J. L. Jerden, *J. Nucl. Mater.*, 2016, **470**, 307–326.
19 B. Lee, Y.-P. Chen, J. Park and J. Park, *ACS Appl. Mater. Interfaces*, 2019, **11**, 25817–25823.
20 N. R. Soelberg, T. G. Garn, M. R. Greenhalgh, J. D. Law, R. Jubin, D. M. Strachan and P. K. Thallapally, *Sci. Technol. Nucl. Install.*, 2013, **2013**, 702496.
21 S. K. Elsaidi, M. H. Mohamed, A. S. Helal, M. Galanek, T. Pham, S. Suepaul, B. Space, D. Hopkinson, P. K. Thallapally and J. Li, *Nat. Commun.*, 2020, **11**, 3103.
22 S. Fajal, W. Mandal, S. Mollick, Y. D. More, A. Torris, S. Saurabh, M. M. Shirolkar and S. K. Ghosh, *Angew. Chem., Int. Ed.*, 2022, e202203385.
23 S. Xiong, X. Tang, C. Pan, L. Li, J. Tang and G. Yu, *ACS Appl. Mater. Interfaces*, 2019, **11**, 27335–27342.
24 J. Wang, K. Ai and L. Lu, *J. Mater. Chem. A*, 2019, **7**, 16850–16858.
25 C. Feng, G. Xu, W. Xie, S. Zhang, C. Yao and Y. Xu, *Polym. Chem.*, 2020, **11**, 2786–2790.
26 M. Outokesh, A. Saket, S. J. Ahmadi, M. Hosseinpour and A. R. Khanchi, *Ind. Eng. Chem. Res.*, 2012, **51**, 15315–15323.

27 M. H. Choi, H.-E. Shim, S.-J. Yun, S.-H. Park, D. S. Choi, B.-S. Jang, Y. J. Choi and J. Jeon, *ACS Appl. Mater. Interfaces*, 2016, **8**, 29227–29231.
28 T. Geng, C. Zhang, M. Liu, C. Hu and G. Chen, *J. Mater. Chem. A*, 2020, **8**, 2820–2826.
29 Y. H. Abdelmoaty, T.-D. Tessema, F. A. Choudhury, O. M. El-Kadri and H. M. El-Kaderi, *ACS Appl. Mater. Interfaces*, 2018, **10**, 16049–16058.
30 S. Das, P. Heasman, T. Ben and S. Qiu, *Chem. Rev.*, 2017, **117**, 1515–1563.
31 S. Fajal, W. Mandal, D. Majumder, M. M. Shirolkar, Y. D. More and S. K. Ghosh, *Chem. – Eur. J.*, 2022, **28**, e202104175.
32 L. Zou, Y. Sun, S. Che, X. Yang, X. Wang, M. Bosch, Q. Wang, H. Li, M. Smith, S. Yuan, Z. Perry and H.-C. Zhou, *Adv. Mater.*, 2017, **29**, 1700229.
33 T. Islamoglu, Z. Chen, M. C. Wasson, C. T. Buru, K. O. Kirlikovali, U. Afrin, M. R. Mian and O. K. Farha, *Chem. Rev.*, 2020, **120**, 8130–8160.
34 T. Zhang, G. Xing, W. Chen and L. Chen, *Mater. Chem. Front.*, 2020, **4**, 332–353.
35 D. Taylor, S. J. Dalgarno, Z. Xu and F. Vilela, *Chem. Soc. Rev.*, 2020, **49**, 3981–4042.
36 D. Chen, C. Liu, J. Tang, L. Luo and G. Yu, *Polym. Chem.*, 2019, **10**, 1168–1181.
37 Q.-Q. Dang, X.-M. Wang, Y.-F. Zhan and X.-M. Zhang, *Polym. Chem.*, 2016, **7**, 643–647.
38 N. Baig, S. Shetty, S. Al-Mousawi and B. Alameddine, *Polym. Chem.*, 2021, **12**, 2282–2292.
39 A. Hassan, S. Goswami, A. Alam, R. Bera and N. Das, *Sep. Purif. Technol.*, 2021, **257**, 117923.
40 W. Mandal, S. Fajal, S. Mollick, M. M. Shirolkar, Y. D. More, S. Saurabh, D. Mahato and S. K. Ghosh, *ACS Appl. Mater. Interfaces*, 2022, **14**, 20042–20052.
41 J. L. Segura, M. J. Mancheño and F. Zamora, *Chem. Soc. Rev.*, 2016, **45**, 5635–5671.
42 R. Dawson, A. I. Cooper and D. J. Adams, *Prog. Polym. Sci.*, 2012, **37**, 530–563.
43 Y. Jin, Y. Zhu and W. Zhang, *CrystEngComm*, 2013, **15**, 1484–1499.
44 Z. Guo, P. Sun, X. Zhang, J. Lin, T. Shi, S. Liu, A. Sun and Z. Li, *Chem. – Asian J.*, 2018, **13**, 2046–2053.
45 P. Wang, Q. Xu, Z. Li, W. Jiang, Q. Jiang and D. Jiang, *Adv. Mater.*, 2018, **30**, 1801991.
46 X. Pan, X. Qin, Q. Zhang, Y. Ge, H. Ke and G. Cheng, *Microporous Mesoporous Mater.*, 2020, **296**, 109990.
47 S. Zhang, X. Li, W. Gong, T. Sun, Z. Wang and G. Ning, *Ind. Eng. Chem. Res.*, 2020, **59**, 3269–3278.
48 Y. Yang, X. Xiong, Y. Fan, Z. Lai, Z. Xu and F. Luo, *J. Solid State Chem.*, 2019, **279**, 120979.
49 Y. Sun, S. Song, D. Xiao, L. Gan and Y. Wang, *ACS Omega*, 2020, **5**, 24262–24271.
50 S. An, X. Zhu, Y. He, L. Yang, H. Wang, S. Jin, J. Hu and H. Liu, *Ind. Eng. Chem. Res.*, 2019, **58**, 10495–10502.
51 R. Chen, T. Hu and Y. Li, *React. Funct. Polym.*, 2021, **159**, 104806.
52 G. Deng and Z. Wang, *ACS Appl. Mater. Interfaces*, 2017, **9**, 41618–41627.
53 S. Gu, J. He, Y. Zhu, Z. Wang, D. Chen, G. Yu, C. Pan, J. Guan and K. Tao, *ACS Appl. Mater. Interfaces*, 2016, **8**, 18383–18392.
54 H. Tan, Q. Chen, T. Chen and H. Liu, *ACS Appl. Mater. Interfaces*, 2018, **10**, 32717–32725.
55 M. Ansari, A. Alam, R. Bera, A. Hassan, S. Goswami and N. Das, *J. Environ. Chem. Eng.*, 2020, **8**, 103558.
56 A. Alam, A. Hassan, R. Bera and N. Das, *Mater. Adv.*, 2020, **1**, 3406–3416.
57 K. Zhao, L. Kong, W. Yang, Y. Huang, H. Li, S. Ma, W. Lv, J. Hu, H. Wang and H. Liu, *ACS Appl. Mater. Interfaces*, 2019, **11**, 44751–44757.
58 X. Qian, Z.-Q. Zhu, H.-X. Sun, F. Ren, P. Mu, W. Liang, L. Chen and A. Li, *ACS Appl. Mater. Interfaces*, 2016, **8**, 21063–21069.
59 Y. Zhu, Y.-J. Ji, D.-G. Wang, Y. Zhang, H. Tang, X.-R. Jia, M. Song, G. Yu and G.-C. Kuang, *J. Mater. Chem. A*, 2017, **5**, 6622–6629.
60 M. Xu, T. Wang, L. Zhou and D. Hua, *J. Mater. Chem. A*, 2020, **8**, 1966–1974.
61 Y. Chen, H. Sun, R. Yang, T. Wang, C. Pei, Z. Xiang, Z. Zhu, W. Liang, A. Li and W. Deng, *J. Mater. Chem. A*, 2015, **3**, 87–91.
62 X. Guo, Y. Tian, M. Zhang, Y. Li, R. Wen, X. Li, X. Li, Y. Xue, L. Ma, C. Xia and S. Li, *Chem. Mater.*, 2018, **30**, 2299–2308.
63 A. Hassan, A. Alam, M. Ansari and N. Das, *Chem. Eng. J.*, 2022, **427**, 130950.
64 Y. Li, W. Chen, W. Hao, Y. Li and L. Chen, *ACS Appl. Nano Mater.*, 2018, **1**, 4756–4761.
65 W. Du, Y. Qin, C. Ni, W. Dai and J. Zou, *ACS Appl. Polym. Mater.*, 2020, **2**, 5121–5128.
66 M. Thommes, K. Kaneko, A. V. Neimark, J. P. Olivier, F. Rodriguez-Reinoso, J. Rouquerol and K. S. W. Sing, *Pure Appl. Chem.*, 2015, **87**, 1051–1069.
67 C. Wang, Y. Wang, R. Ge, X. Song, X. Xing, Q. Jiang, H. Lu, C. Hao, X. Guo, Y. Gao and D. Jiang, *Chem. – Eur. J.*, 2018, **24**, 585–589.
68 M. H. Choi, S.-W. Jeong, H. E. Shim, S.-J. Yun, S. Mushtaq, D. S. Choi, B.-S. Jang, J. E. Yang, Y. J. Choi and J. Jeon, *Chem. Commun.*, 2017, **53**, 3937–3940.
69 J. Li, H. Zhang, L. Zhang, K. Wang, Z. Wang, G. Liu, Y. Zhao and Y. Zeng, *J. Mater. Chem. A*, 2020, **8**, 9523–9527.
70 X. Hu, H. Wang, C. F. J. Faul, J. Wen, Y. Wei, M. Zhu and Y. Liao, *Chem. Eng. J.*, 2020, **382**, 122998.
71 Y. Liao, J. Weber, B. M. Mills, Z. Ren and C. F. J. Faul, *Macromolecules*, 2016, **49**, 6322–6333.
72 S.-Y. Zhang, X.-H. Tang, Y.-L. Yan, S.-Q. Li, S. Zheng, J. Fan, X. Li, W.-G. Zhang and S. Cai, *ACS Macro Lett.*, 2021, **10**, 1590–1596.
73 H. Zuo, W. Lyu, W. Zhang, Y. Li and Y. Liao, *Macromol. Rapid Commun.*, 2020, **41**, 2000489.
74 L. Xie, Z. Zheng, Q. Lin, H. Zhou, X. Ji, J. L. Sessler and H. Wang, *Angew. Chem., Int. Ed.*, 2022, **61**, e202113724.
75 X. Jiang, X. Cui, A. J. E. Duncan, L. Li, R. P. Hughes, R. J. Staples, E. V. Alexandrov, D. M. Proserpio, Y. Wu and C. Ke, *J. Am. Chem. Soc.*, 2019, **141**, 10915–10923.
76 Y. Lin, X. Jiang, S. T. Kim, S. B. Alahakoon, X. Hou, Z. Zhang, C. M. Thompson, R. A. Smaldone and C. Ke, *J. Am. Chem. Soc.*, 2017, **139**, 7172–7175.